Available online at www.sciencedirect.com

ScienceDirect

Ceramics International 40 (2014) 3139–3144

CERAMICS INTERNATIONAL

www.elsevier.com/locate/ceramint

Electrical properties of niobium doped $Bi_4Ti_3O_{12}$-$SrBi_4Ti_4O_{15}$ intergrowth ferroelectrics

Geetanjali Parida[1], J. Bera*

Department of Ceramic Engineering, National Institute of Technology, Rourkela, Odisha 769008, India

Received 23 September 2013; received in revised form 28 September 2013; accepted 28 September 2013
Available online 7 October 2013

Abstract

Nb-doped $Bi_4Ti_3O_{12}$-$SrBi_4Ti_4O_{15}$ intergrowth ceramics have been prepared by modified oxalate route. XRD phase analysis confirmed the formation of single phase compound. Nb-doping does not affect the basic crystal structure of the intergrowth. SEM micrographs showed that the grain size of the ceramics decreases with Nb-doping. The temperature dependence of dielectric constant and losses was investigated in the temperature range 30–800 °C and frequency range 1 kHz–1 MHz. With Nb-doping, the T_c of the ferroelectrics reduces and peak permittivity increases. Doping also introduces small relaxor behavior in the ferroelectrics. The dc conductivity of the ceramics decreases with doping. The remnant polarization (P_r) of the intergrowth ferroelectrics is increased with Nb doping.

Keywords: B. Defects; B. X-ray methods; C. Electrical properties; C. Ferroelectric properties

1. Introduction

Bismuth layered structure ferroelectrics (BLSFs), referred as Aurivillius phases, have attracted considerable attention for their potential applications in non-volatile memories and high temperature piezoelectric devices [1–3]. They have excellent fatigue free behavior [1]. Moreover, they have environmentally friendly lead free compositions. BLSF crystal structure has layers of bismuth oxide and pseudo perovskite block stacked alternately along their *c*-direction [4,5]. The structure can be represented as $(Bi_2O_2)^{2+}(A_{m-1}B_mO_{3m+1})^{2-}$, where *A* can be mono, di or trivalent ions or mixer of them at 12-coordinated site, *B* may be tetra, penta or hexavalent cations at 6-coordinated site, *m* is the number of BO_6 octahedra in pseudo perovskite blocks.

For commercial application, numerous efforts have been made to improve the electrical properties of BLSFs. Some effective approaches are**:** (i) doping at *A*-site, (ii) high valent cation doping at *B*-site and (iii) formation of intergrowth between different BLSFs. The intergrowth BLSFs are consist of regular stacking of one half the unit cell of *m*-member structure and one half the unit cell of $(m+1)$ member BLSF structure along their *c*-axis [6,7]. For example, the mixed layer BLSF intergrowth $SrBi_7Ti_8O_{27}$ consists of one half the unit cell of 3-layer $Bi_4Ti_3O_{12}$ (BIT) and 4-layer $SrBi_4Ti_4O_{15}$ (SBTi) respectively. These intergrowths have interesting and superior ferroelectric properties compare to their individual compounds. For example, BIT-SBTi intergrowth has an enhanced remnant polarization (P_r) than either BIT or SBTi [8,9]. In general, the polarization in BLSF arises due to the shifting of *A*-type cation along the *a*-axis. However, BIT has a small *c*-axis polarization component in addition to a large *a*-axis component. Thus, intergrowth formation with BIT may be responsible for the enhanced P_r in mixed layer BIT-SBTi compound.

In spite of several advantages of BLSFs, they are still not commercially applicable as they have high leakage current due to the presence of defects like oxygen and bismuth ion vacancies. Volatilization of bismuth during high temperature sintering of BLSFs is an inherent problem, which generates oxygen vacancies to compensate the charge. Many efforts have been made to solve this through donor-doping of cations like Nb^{5+}, V^{5+}, W^{6+} at *B*-site of BLSFs [10–17]. Nb^{5+} doping

*Corresponding author. Tel.: +91 661 2462204; mobile: +91 9437246159.
E-mail addresses: geeta.lily@gmail.com (G. Parida), jbera@nitrkl.ac.in (J. Bera).
[1]Tel.: +91 9178510270.

0272-8842/$ - see front matter © 2013 Elsevier Ltd and Techna Group S.r.l. All rights reserved.
http://dx.doi.org/10.1016/j.ceramint.2013.09.131

in BLSFs is very effective for compensating oxygen vacancies, which reduce dielectric losses [10–12]. It has been reported that the ferroelectric properties of BIT were enhanced by Nb doping [13]. Hou et al. [14] reported that Nb/Ta doping at *B*-site of BIT caused a remarkably suppressed grain growth, increased permittivity and piezoelectric activity. Bobić et al. [15] reported an increase of the degree of diffuseness of the dielectric peak in $BaBi_4Ti_4O_{15}$ (BBTi) with Nb-doping. A considerable remnant polarization and excellent fatigue-endurance properties were reported in V-doped SBTi thin film [16].

Currently there are very few reports [9,18] related to such kind of *B*-site donor-doping in BIT-SBTi ceramics. Wang et al. [9] reported that the remnant polarization of tungsten-doped BIT-SBTi intergrowth ceramics was over twice as large as that of non-doped one, when *W* content was 0.03. Same group [18] further reported that the remnant polarization and piezoelectric properties of BIT-SBTi were greatly increased by Nb and V doping. In the present investigation Nb^{5+} has been doped in *B*-site of BIT-SBTi intergrowth and the effect of the doping in crystal structure, microstructure, dielectric and ferroelectric properties of the intergrowth ferroelectrics, was investigated.

2. Experimental procedure

$Bi_4Ti_{3-x}Nb_xO_{12}$–$SrBi_4Ti_{4-x}Nb_xO_{15}$ intergrowth ceramics with $x=0.04$, 0.06 and 0.08 (will be presented as BTN-SBTN$_x$) were synthesized by the modified oxalate route reported recently [19]. Briefly, strontium nitrate ($Sr(NO_3)_2$), bismuth nitrate ($Bi(NO_3)_3\cdot 5H_2O$), titanium dioxide (TiO_2), niobium pentoxide (Nb_2O_5) and oxalic acid ($C_2H_2O_4\cdot 2H_2O$) were used as raw materials for the synthesis. Required amount of $Bi(NO_3)_3\cdot 5H_2O$ and $Sr(NO_3)_2$ was dissolved in minimum quantity of concentrated nitric acid and in water, respectively. Bismuth nitrate solution was then added drop wise to strontium nitrate solution under stirring condition. Required amount of TiO_2 and Nb_2O_5 was dispersed in 0.4 M oxalic acid solution. Bismuth and strontium nitrate mixed solution was then added drop by drop into the oxalic acid-oxide particle suspension under vigorous stirring. Bismuth oxalate hydrate and strontium oxalate hydrate were precipitated in the suspension through heterogeneous nucleation. Finally, the pH of the suspension was adjusted to 7 using ammonium hydroxide. The precipitated mixture was separated from the solution by filtration and was washed thoroughly, followed by drying at 50 °C for 24 h to get the precursor powder for intergrowth ceramics synthesis.

The precursor powder was calcined at 800 °C for 4 h for three times with intermediate grinding after each firing to get pure phase BIT-SBTi powder. The BIT-SBTi powder was compressed into pellet at 220 MPa using hydraulic press. The pellets were then sintered at 1150 °C for 2 h. The phase identification was performed using powder X-ray diffraction (XRD) patterns obtained in Philips PW-1830 diffractometer. The lattice parameters and other structural information were evaluated through Rietveld refinement of XRD pattern. The surface morphology of the sintered specimen was studied using field emission scanning electron microscope (FE-SEM) NANO-NOVA, FEI. For electrical measurements, sintered pellets were coated with silver paint electrodes and cured at 700 °C. The frequency dependence of the dielectric constant and loss tangent was measured using a Solatron 1260 Impedance Grain/Phase analyzer in the temperature range 30 to 800 °C and frequency range 1 kHz–1 MHz. The ferroelectric polarization-electric field (*P*–*E*) loops were measured at room temperature using a ferroelectric hysteresis tracer by applying 50 Hz frequency.

3. Results and discussion

Fig. 1 shows the XRD patterns of Nb doped BIT-SBTi ceramics. All patterns have single phase and were matched with standard PDF File no. 31-1342 for the compound $SrBi_8Ti_7O_{27}$. The compound $SrBi_8Ti_7O_{27}$ has $Bi_4Ti_3O_{12}$ plus $SrBi_4Ti_4O_{15}$ mixed layered intergrowth structure. The diffraction peaks were indexed according to this standard powder diffraction data. Similar XRD patterns were reported earlier [8,9] for BIT-SBTi intergrowth ceramics. XRD results indicate that Nb-doping does not affect the basic crystal structure of intergrowth ceramics. Only, there was little shifting of diffraction peaks towards lower 2-theta angle with Nb doping. Lattice parameters of intergrowth ceramics were refined by the Rietveld method using MAUD program [20], considering orthorhombic space group *I2cm* (SG No 46: *-cba*). The space group was reported by Tellier et al. [21] for similar intergrowth compound $PbBi_8Ti_7O_{27}$. This space group requires a doubling of the usual *c*-parameter ~37 Å. Refined lattice parameters and unit cell volume of different compositions are listed in Table 1. Since the ionic radii of Nb^{5+} (0.0640 nm) is close to that of Ti^{4+} (0.0605 nm) [22], there was very little change in unit cell volume at low concentration of Nb-doping. However, a slight increase of cell volume in BTN-SBTN$_{0.08}$ may be due

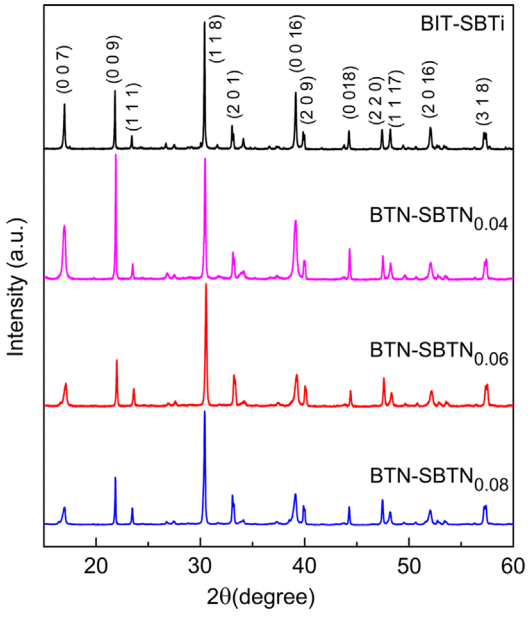

Fig. 1. X-ray diffraction patterns of BIT-SBTi, BTN-SBTN$_{0.04}$, BTN-SBTN$_{0.06}$ and BTN-SBTN$_{0.08}$ ceramics.

Table 1
Percent theoretical density, lattice parameters; a, b, c in Å, volume of unit cell in (Å)^3, and March-Dollase texture factor for different composition (x) in BTN-SBTN$_x$ intergrowth ceramics.

x	% theoretical density	a (Å)	b (Å)	c (Å)	Volume of unit cell (Å)^3	Texture factor
0.00	92	5.4332(1)	5.4145(3)	73.7316(8)	2169	0.65
0.04	93	5.4262(3)	5.4221(1)	73.7911(6)	2171	0.58
0.06	95	5.4305(2)	5.4229(4)	73.8706(7)	2175	0.76
0.08	95	5.4454(2)	5.4399(3)	74.1221(9)	2196	0.77

to increased concentration of doping. Similar increase of lattice parameters in SBTi was reported by Hao et al. [23] at higher concentration of Nb-doping.

Diffraction patterns show that there are preferred orientations of (00l) peaks in pure and BTN-SBTN$_{0.04}$ ceramics, which is due to the preferential growth of plate like grain in BLSF ceramics. As they have highly anisotropic crystal structure with longer c-axis compared to a and b, the {00l} planes possess lower surface energy, resulting in a rapid grain growth in the a–b plane during sintering. The preferred orientation can be quantified by determining the texture factor in Rietveld analysis. March–Dollase texture factors refined for each composition are listed in Table 1. For completely random distribution of grains, the texture factor value equals to 1 (one) and the factor will be less than unity for plate-like grains. The preferred orientation was highest in BTN-SBTN$_{0.04}$ ceramics as the factor was lowest ~0.58. However, the preferred orientation decreases with further increase in Nb. This is due to the fact that Nb acts as a grain growth inhibitor during sintering [15].

All compositions were sintered to more than 90% of their theoretical density (Table 1). There is little improvement in density with Nb-doping. Similar improvement in density of BBTi has also been reported [15] upon Nb doping. Fig. 2 shows surface morphology of some selected composition, namely pure BIT-SBTi and BTN-SBTN$_{0.08}$ ceramics. It shows typical plate-like grains in both. The average thickness and diameter of the plates were 0.6 and 3.5 μm respectively in pure BIT-SBTi and 0.36, 2.0 μm respectively in BTN-SBTN$_{0.08}$ ceramics. This indicates that the grain size and thickness decrease with Nb-doping. It has been reported that Nb-doping acts as a grain growth inhibitor in different BLSFs [11,15]. An improvement of density with Nb doping may be due to the decrease in grain size with doping [15].

Fig. 3 shows the temperature dependence of dielectric constant (ε') and dielectric loss (tan δ) measured at a frequency of 100 kHz for pure and Nb doped BIT-SBTi. The Curie temperatures (T_c) of different compositions are shown in Table 2. The T_c of pure BIT-SBTi is at 610 °C and it nominally decreases to 580 °C when Nb doping was 0.08. This indicates that the Nb doping at B-site affects very little on the shifting of T_c. In Aurivillius compound, the shifting of T_c is related to the distortion of lattice [24] and T_c decreases with the decrease in distortion. There was a small decrease in orthorhombicity of the structure with Nb-doping as shown in Table 2. The orthorhombicity of the structure is represented

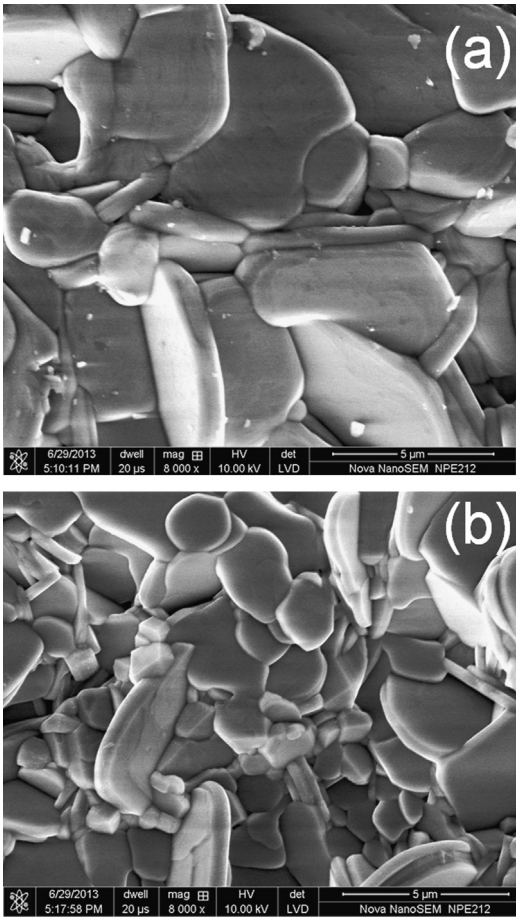

Fig. 2. Surface morphology of BIT-SBTi (a) and BTN-SBTN$_{0.08}$ and (b) ceramics.

by [2(a−b)]/(a+b). Decreased orthorhombicity is due to the decreased distortion of the structure. A small decrease in T_c with Nb doping may be due to this decreased distortion of the structure. So the Nb^{5+} doping for Ti^{4+} causes a negligible change in lattice distortion.

Fig. 3 also shows that the peak permittivity increases and the peaks become broader with Nb doping. Peak permittivity increases due to increased densification and decreased preferred orientation of ceramics with Nb doping. Also, Nb is ferroelectrically more active than Ti. The similar peak broadening in Nb doped BIT has been reported earlier [12]. The broadness of permittivity peak originates from the compositional fluctuation in crystallographic sites when one or more cations occupy the same site in the structure [25]. There is no

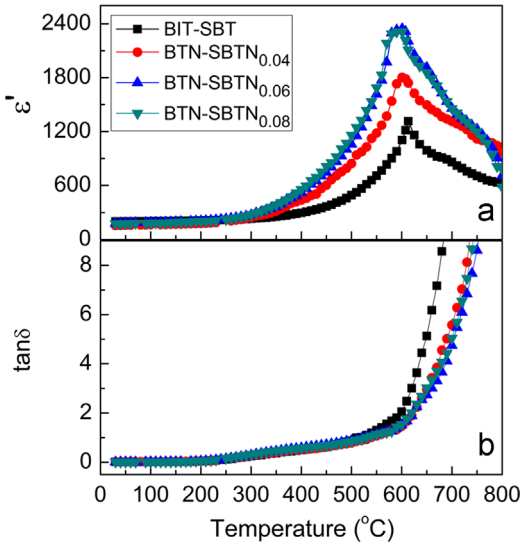

Fig. 3. Temperature dependence of dielectric permittivity (a) and loss (b) for BIT-SBTi, BTN-SBTN$_{0.04}$, BTN-SBTN$_{0.06}$ and BTN-SBTN$_{0.08}$ ceramics.

Table 2
The temperature of dielectric maximum (T_c) measure at 100 kHz, orthorhombicity, the degree of diffuseness (γ) and activation energy for dc conductivity (E_{dc}) of different compositions (x) in BTN-SBTN$_x$ intergrowth ceramics.

x	T_c (°C)	Orthorhombicity	γ	E_{dc}
0.00	610	0.0034	0.96	1.00
0.04	600	0.0010	0.98	1.02
0.06	590	0.0014	1.23	1.07
0.08	580	0.0010	1.27	1.12

dielectric loss relaxation peak in the tan δ–temperature curve. At room temperature, the dielectric losses were comparable for all compositions. Above about 600 °C, there is a sudden increase of tan δ in all composition due to the increase in thermally assisted conductive current. Pure BIT-SBTi ceramics show higher dielectric losses compared to Nb-dope ceramics due to the presence of more oxygen vacancies in un-doped ceramics.

It has been stated above that the ferroelectric to paraelectric phase transition peak become broader and diffuse with Nb doping. The diffuseness of the phase transition can be described using modified Curie–Weiss law:

$$(1/\varepsilon' - 1/\varepsilon'_m) = [(T - T_m)^\gamma]/C \quad \text{for } (T > T_m) \tag{1}$$

where C is the modified Curie–Weiss constant and γ indicates the degree of diffuseness of the phase transition. The value of γ lies in the range $1 \le \gamma \le 2$; in case of normal ferroelectric, $\gamma = 1$ and for ideal relaxors, $\gamma = 2$. The values of γ calculated for different compositions are shown in Table 2. The γ value increases gradually from 0.96 to 1.27 with Nb doping. This indicates that the doping changes the ferroelectric behavior from normal to a relaxor type in BIT-SBTi ceramics. Jenneta et al. [26] reported a similar change of ferroelectric properties of BIT upon Nb doping. This phenomenon is correlated to the relaxation of polar clusters induced by hetero-valent Nb^{5+} at B-site.

One of the most important electrical properties of ferroelectrics is the dc conductivity due to vacancy conduction. The activation energy for that vacancy conduction can be evaluated from complex impedance (Cole–Cole) plot. Fig. 4(a) and (b) shows the temperature dependence of the complex impedance spectra for pure BIT-SBTi and BTN-SBTN$_{0.08}$ ceramics, respectively. The intercepts of the semi-circular arc on real axis gives the total resistance (R_{tot}). Using R_{tot}, dc conductivity (σ_{dc}) of the bulk can be evaluated using the relation; $\sigma_{dc} = t/(R_{tot}A)$, where t and A are the thickness and area of the pellet, respectively. The activation energy (E_{dc}) for the dc conductivity can be calculated from the Arrhenius equation; $\sigma_{dc} = \sigma_0 \exp[-E_{dc}/(k_B T)]$, using the slope of the plot of log σ_{dc} versus inverse of temperature (T) as is shown in inset of Fig. 4(a) and (b), respectively. The activation energy E_{dc}, calculated for all the compositions are listed in Table 2. E_{dc} increases with the increase in Nb doping. This implies that the amount of oxygen vacancies decreases with increase in donor doping.

It is known that the point defects i.e. oxygen vacancy play an important role in electrical properties of ferroelectric ceramics. The substitution of higher valent cation at B-site decreases the concentration of oxygen vacancies as per defect reaction;

$$Nb_2O_5 \leftrightarrow 2Nb_{Ti}\bullet + 5O_O + 2e' \tag{2}$$

$$\S O_2(\mathbf{g}) + V_O\bullet\bullet + 2e' \leftrightarrow O_O \tag{3}$$

Nb doping produces 2 numbers of Nb_{Ti} holes and 2 electrons. Theses 2 electrons combine with 1 oxygen atom, can offset an oxygen vacancy, resulting the decrease in oxygen vacancy concentration.

Fig. 5 represents the polarization with the electric field (P–E) hysteresis loop of BTN-SBTN$_{0.06}$ and pure BIT-SBTi ceramic under the applied electric field 32 KV/cm. Both the curves are minor loops and they are not saturated due to the limitation of the applicable electric field of the equipment and room temperature measurement. However, they can be compared. The $2P_r$ of BTN-SBTN$_{0.06}$ is higher than pure BIT-SBTi and was highest among all compositions studied. It is known that oxygen vacancy space charges act as a domain pinning centers and reduces polarization. The increased $2P_r$ of Nb doped ceramics may be due to the reduced oxygen vacancy in doped ceramics.

4. Conclusions

Nb-doped $Bi_4Ti_3O_{12}$–$SrBi_4Ti_4O_{15}$ mixed layer intergrowth ceramics has been successfully synthesized through modified oxalate route at a temperature of 800 °C. XRD analysis showed that the Nb-doping does not affect the basic crystal structure, except small increase in lattice parameters. The preferred orientation of plate-like grains and their sizes decreased with Nb-doping. This indicates that Nb acts as a grain growth inhibitor. The T_c of the intergrowth ferroelectrics

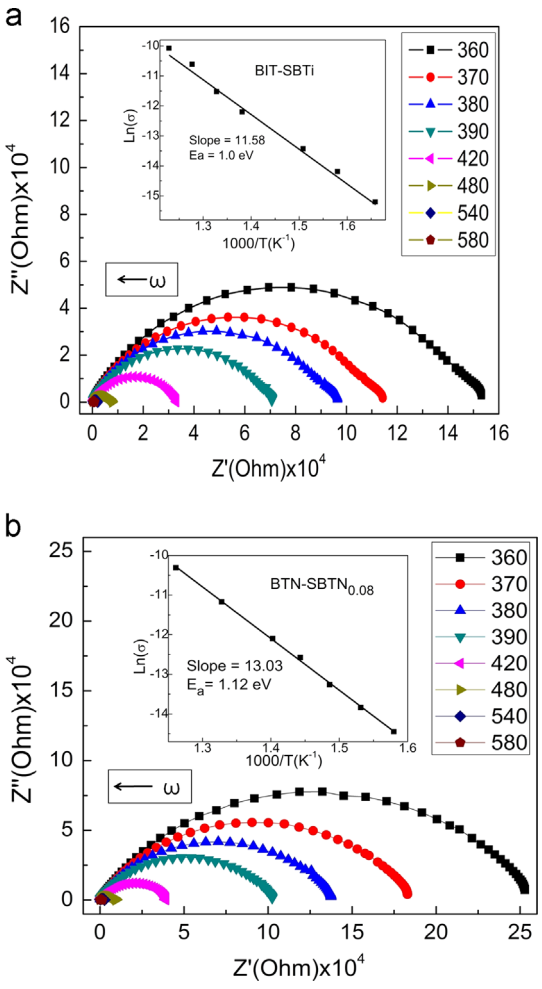

Fig. 4. Complex impedance plot of BIT-SBTi (a) and BTN-SBTN$_{0.06}$ (b) ceramics at different temperatures. Insets are the Arrhenius plots of dc conductivity of respective ceramics.

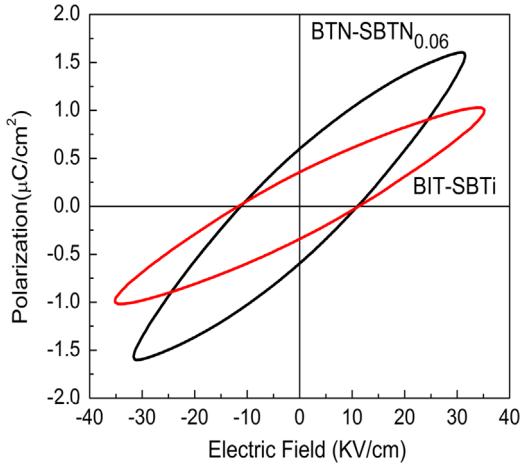

Fig. 5. *P–E* hysteresis loops for BIT-SBTi (a) and BTN-SBTN$_{0.06}$ (b) ceramics.

decreases due to the decrease in orthorhombicity of the structure and hence, distortion of the structure. The peak permittivity of the intergrowth ferroelectrics increases due to the increase in density and decrease in preferred orientation of plate-like grains with Nb doping. Doping also introduces small relaxor behavior in the ceramics. The dc conductivity of ceramics decreases with doping. The remnant polarization (P_r) of the intergrowth compound is increased due to decreased oxygen vacancy concentration with Nb doping.

Acknowledgments

This research was financially supported by National Institute of Technology, Rourkela, India.

References

[1] B.H. Park, B.S. Kang, S.D. Bu, T.W. Noh, J. Lee, W. Jo, Lanthanum-substituted bismuth titanate for use in non-volatile memories, Nature 401 (1999) 682–684.
[2] X. Wang, Method for manufacturing piezoelectric film element, United States Patent, 2011 Pub. No. US 2011/7872403 B2.
[3] M. Furukaw, D. Tanaka, T. Takenaka, H. Nagata, H. Hiruma, Piezoelectric composition, Piezoelectric Ceramic, Transducer, and Ultrasonic Motor, United States Patent, 2011 Pub. No. US 2011/0241483 A1.
[4] B. Aurivillius, Mixed bismuth oxide with layer lattices II Structure of $Bi_4Ti_3O_{12}$, Arkiv fur Kemi 1 (1949) 499–512.
[5] B.T. Matthias, Ferroelectricity, Science 113 (1951) 591–596.
[6] T. Kikuchi, Synthesis of a new, mix-layered bismuth titanate $SrBi_8Ti_7O_{27}$, Journal of the Less Common Metals 52 (1977) 163–165.
[7] T. Kikuchi, A. Watanabe, K. Uchida, A family of mixed-layer type bismuth compounds, Materials Research Bulletin 12 (1977) 299–304.
[8] Y. Noguchi, M. Miyayama, T. Kudo, Ferroelectric properties of intergrowth $Bi_4Ti_3O_{12}$–$SrBi_4Ti_4O_{15}$ ceramics, Applied Physics Letters 77 (2000) 3639–3641.
[9] W. Wang, J. Zhu, X.Y. Mao, X.B. Chen, Properties of tungsten-doped $Bi_4Ti_3O_{12}$–$SrBi_4Ti_4O_{15}$ intergrowth ferroelectrics, Materials Research Bulletin 42 (2007) 274–280.
[10] S. Hong, S. Trolier-mckinstry, G.L. Messing, Dielectric and electromechanical properties of textured niobium-doped bismuth titanate ceramics, Journal of the American Ceramic Society 83 (1) (2000) 113–118.
[11] J.K. Kim, J. Kim, T.K. Song, S.S. Kim, Effects of niobium doping on microstructures and ferroelectric properties of bismuth titanate ferroelectric thin films, Thin Solid Films 419 (2002) 225–229.
[12] J.S. Kim, C.W. Ahn, H.J. Lee, I.W. Kim, B.M. Jin, Nb doping effects on ferroelectric and electrical properties of ferroelectric $Bi_{3.25}La_{0.75}(Ti_{1-x}Nb_x)_3O_{12}$ ceramics, Ceramics International 30 (2004) 1459–1462.
[13] S.K. Singh, H. Ishiwara, Ferroelectric properties enhancement in niobium-substituted $Bi_{3.25}La_{0.75}Ti_3O_{12}$ thin films prepared by chemical solution route, Thin Solid Films 497 (2006) 90–95.
[14] J. Hou, R.V. Kumar, Y. Qu, D. Krsmanovic, B-site doping effect on electrical properties of $Bi_4Ti_{3-2x}Nb_xTa_xO_{12}$ ceramics, Scripta Materialia 61 (2009) 664–667.
[15] J.D. Bobić, M.M. Vijatović Petrović, J. Banys, B.D. Stojanović, Electrical properties of niobium doped barium bismuth-titanate ceramics, Materials Research Bulletin 47 (2012) 1874–1880.
[16] H. Sun, J. Zhu, H. Fang, X.B. Chen, Large remnant polarization and excellent fatigue property of vanadium-doped $SrBi_4Ti_4O_{15}$ thin films, Journal of Applied Physics 100 (2006) 074102 (4 pp).
[17] M. Adamczyk, L. Kozielski, M. Pilch, M. Pawełczyk, A. Soszyński, Influence of vanadium dopant on relaxor behavior of $BaBi_2Nb_2O_9$ ceramics, Ceramics International 39 (2013) 4589–4595.
[18] W. Wang, D. Shan, J. Sun, X. Mao, X. Chen, Aliovalent B-site modification on three- and four-layer Aurivillius intergrowth, Journal of Applied Physics 103 (2008) 044102 (7 pp).
[19] G. Parida, J. Bera, Dielectric properties of $Bi_4Ti_3O_{12}$-$SrBi_4Ti_4O_{15}$ intergrowth ceramics synthesized by modified oxalate route, Phase Transitions (2013) ⟨http://dx.doi.org/10.1080/01411594.2013.837465/⟩.
[20] ⟨http://www.ing.unitn.it/∼maud/⟩.

[21] J. Tellier, P. Boullay, D. Mercurio, Crystal structure of the Aurivillius phases in the system $Bi_4Ti_3O_{12}$-$PbTiO_3$, Zeitschrift für Kristallographie 222 (2007) 234–243.

[22] R.D. Shannon, Revised effective ionic radii and systematic studies of interatomic distances in halides and chalcogenides, Acta Crystallographica A32 (1976) 751–767.

[23] H. Hao, H. Liu, S. Ouyang, Structure and ferroelectric property of Nb-doped $SrBi_4Ti_4O_{15}$ ceramics, Journal of Electroceramics 22 (2009) 357–362.

[24] D.Y. Suarez, I.M. Reaney, W.E. Lee, Relation between tolerance factor and T_c in Aurivillius compounds, Journal of Materials Research 16 (2001) 3139–3149.

[25] J. Tellier, Ph. Boullay, M. Manier, D. Mercurio, A comparative study of the Aurivillius phase ferroelectrics $CaBi_4Ti_4O_{15}$ and $BaBi_4Ti_4O_{15}$, Journal of Solid State Chemistry 177 (2004) 1829–1837.

[26] D.B. Jennet, P. Marchet, M. El Maaoui, J.P. Mercurio, From ferroelectric to relaxor behavior in the Aurivillius-type $Bi_{4-x}Ba_xTi_{3-x}Nb_xO_{12}$ ($0 \leq x \leq 1.4$) solid solutions, Materials Letters 59 (2005) 376–382.